

Article

Ensemble Projection of Future Climate and Surface Water Supplies in the North Saskatchewan River Basin above Edmonton, Alberta, Canada

Muhammad Rehan Anis * and David J. Sauchyn

The Prairie Adaptation Research Collaborative, University of Regina, Suite 219-2 Research Drive, 3737 Wascana Parkway, Regina, SK S4S 0A2, Canada; sauchyn@uregina.ca

* Correspondence: rehan.anis@uregina.ca; Tel.: +1-(306)-250-5773

Abstract: Changes in temperature and precipitation are expected to alter the seasonal distribution of surface water supplies in snowmelt-dominated watersheds. A realistic assessment of future climate change and inter-annual variability is required to meet a growing demand for water supplies in all major use sectors. This study focuses on changes in climate and runoff in the North Saskatchewan River Basin (NSRB) above Edmonton, AB, Canada, using the MESH (Modélisation Environnementale communautaire—Surface Hydrology) model. The bias-corrected ensemble of Canadian Regional Climate Model (CanRCM4) data is used to drive MESH for two 60-year time periods, a historical baseline (1951–2010) and future projection (2041–2100), under Representative Concentration Pathway (RCP) 8.5. The precipitation is projected to increase in every season, there is significant trend in spring (0.62) and fall (0.41) and insignificant in summer (0.008). Winter extreme minimum temperature and summer extreme maximum temperature are increasing by 2–3 °C in the near future and 5–6 °C in the far future. Annual runoff increases by 19% compared to base period. The results reveal long-term hydrological variability enabling water resource managers to better prepare for climate change and extreme events to build more resilient systems for future water demand in the NSRB.

Keywords: ensemble modeling; land surface hydrological model; climate change; extreme runoff change



Citation: Anis, M.R.; Sauchyn, D.J. Ensemble Projection of Future Climate and Surface Water Supplies in the North Saskatchewan River Basin above Edmonton, Alberta, Canada. *Water* **2021**, *13*, 2425. <https://doi.org/10.3390/w13172425>

Academic Editor: Aizhong Ye

Received: 9 July 2021

Accepted: 31 August 2021

Published: 3 September 2021

Publisher's Note: MDPI stays neutral with regard to jurisdictional claims in published maps and institutional affiliations.



Copyright: © 2021 by the authors. Licensee MDPI, Basel, Switzerland. This article is an open access article distributed under the terms and conditions of the Creative Commons Attribution (CC BY) license (<https://creativecommons.org/licenses/by/4.0/>).

1. Introduction

A shift in the seasonal distribution of surface water supplies, and in the frequency and severity of flooding and drought, are among the most problematic regional impacts of global climate change [1–3]. These impacts are especially challenging in water-limited landscapes and where watershed hydrology is dominated by the melt of a cold season snowpack. Both of these geographic characteristics apply to the mid- and high-latitude snow-dominated river basins of western Canada. This region has also been subject to considerable climate change. Since 1948, Canada has warmed at twice the global rate; while in western Canada, the increase in temperature has been about three times more rapid than global warming [4,5]. As a result, the flow of rivers draining the eastern slopes of the Canadian Rocky Mountains has declined in recent decades [6–12].

Over the same period, there has been a growing demand for water supplied from the Rocky Mountains of western Alberta. This province has a population of about 4.3 million. It also has most of Canada's oil and gas industry and irrigated agricultural land. While the Rocky Mountains are the water towers of the western interior, most of Alberta is sub-humid, with large seasonal and inter-annual variability and extreme weather typical of a mid-latitude continental climate. Out of the 20 most damaging weather events in Canadian history, 16 occurred in Alberta [13].

Alberta's capital city, Edmonton, is the fifth most populous urban area in Canada with about 1.4 million residents. The water supply for this metropolitan region is the North Saskatchewan River (NSR). The headwater tributaries (Cline, Brazeau, Ram, and

Clearwater rivers) generate 88% of the total annual runoff [14]. Melt of the high elevation snowpack maintains river flow through the summer months. At Edmonton, the average annual temperature has risen by more than 2 °C over the past 120 years. Most of this climate change has been an increase in the lowest temperatures; minimum daily winter temperatures have increased by 6 °C [15]. A decrease in the average annual flow of the NSR at Edmonton since 1911 is consistent with a warmer climate and the resulting loss of snowpack at high elevations in the headwaters of the river basin. However, the decline is small compared to large natural inter-annual and decadal variability in flow. Most of the decreased flow is in summer; winter flows have been trending upward [15].

Previous studies of the impacts of climate change on runoff in the NSRB have applied coarse output from Global Climate Models (GCMs) to a hydrological model [16] or taken runoff data directly from simple simulations of hydrology embedded in Regional Climate Models (RCMs) [9]. The objective of the research described here was to inform water supply and adaptation planning for climate change in the Edmonton region with an innovative and higher-resolution approach to modeling of the climate and hydrology of the NSRB. We processed outputs from a 15-member ensemble of runs of the Canadian Regional Climate Model (version CanRCM4). Then, we ran a fully calibrated, high-resolution (10 km) hydrological model, using the future climatology from CanRCM4 and the RCP8.5 greenhouse gas concentration pathway. This ensemble approach enables us to capture uncertainty resulting from the natural variability of the regional hydroclimate, and control for uncertainty related to the use of different climate models and emission scenarios.

The quantification of climate uncertainty in the ensemble-based predictions of hydrological impact is necessary for the devising of a robust future water demand strategy. An ensemble of hydrographs under future climate conditions, and information about the future timing and magnitude of extreme water levels, informs a climate risk assessment of the resilience of water resource policy and infrastructure, which was designed to operate under the historical climatic variability. Human-induced climate trends are superimposed on natural climatic variability, which is more evident and impactful at regional scales. Inter-annual and decadal-scale variability of the regional hydroclimate is the dominant source of uncertainty in the projection of the future climate of Canada's western interior [17]. Our interpretation of the future contribution of natural variability is very much guided by our prior reconstruction of the flow of the NSR from tree rings [18–20]. This 900-year record of hydroclimatic variability includes evidence of prolonged periods of low flows exceeding in severity and duration the minimum flows in the gauge record.

Anis et al. [15] provided an overview of the impacts of climate change on water security in Canada's western interior with a focus on the NSRB. That book chapter took a broad view, including reviews of historical changes in climate and hydrology, the paleohydrology of the past millennium, and data on water use and demand of past and future decades. This paper, on the other hand, is focused exclusively on the projected changes in climate and river flow in the NSRB above Edmonton, AB, Canada, with technical details and results not included in [15].

2. MESH Model and Input Data

2.1. Study Area

Above Edmonton, the NSRB has a drainage area of 28,100 km² and elevations ranging between 611 and 3543 m above sea level. Three major physiographic regions—the Rocky Mountains, foothills, and plains—are evident from the elevations in Figure 1a and land cover image of the basin in Figure 1b. The lower mountain slopes have a cover of montane and sub-alpine forests. The foothill's vegetation is temperate needleleaf and mixed forest. The plains land cover is primarily crops and temperate grassland, with some broadleaf deciduous forest (aspen parkland). While the sub-humid plains comprise about 60 percent of the drainage area, they contribute a small amount of discharge to the North Saskatchewan River (NSR).

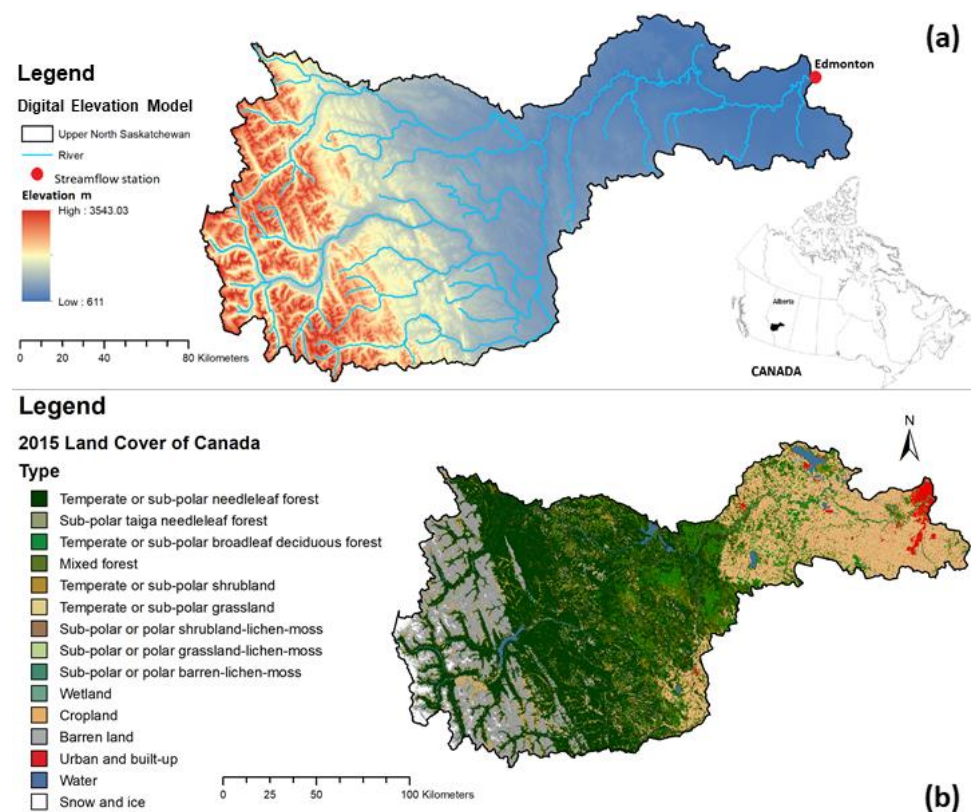


Figure 1. (a) The physiography and river network of the NSRB. (b) Land cover classification of NSRB above Edmonton, AB, Canada.

The average annual precipitation across the entire drainage area is 619.5 mm (1979–2016); however, it varies from about 475 mm at Edmonton to more than 1000 mm in the Rocky Mountain ranges. The average annual (1979–2016) minimum and maximum temperatures over this region are -12.3 and 13.6 °C, respectively. Temperatures also vary significantly between the mountains and the plains. The mean annual discharge of the NSR above Edmonton is around $215 \text{ m}^3/\text{s}$. The origin of the NSR is the Saskatchewan Glacier in the Columbia Icefields. The glaciers of the Columbia Icefield lost about 22.5% of their total area from 1919 to 2009 [21].

2.2. MESH Land Surface Hydrological Model

The hydrology of the NSRB above Edmonton was simulated using the MESH modeling system. MESH is a semi-distributed hydrological land-surface scheme developed by Environment and Climate Change Canada [22]. It has three components:

1. The Canadian Land Surface Scheme (CLASS) [23,24] calculates the energy and water balances using physically-based equations for snow, soil, and vegetation at a 30 min time step;
2. The routing scheme for the inter-grid transfer of channel flow (lateral movement) between surface water and soil to the drainage system with the option of using a algorithm PDMROF [25] or WATROF [26];
3. The hydrological routing, using the semi-distributed hydrological model WATFLOOD [27], accumulates overland flow and interflow from each grid cell at a given time step and routes them through the drainage system to the basin outlet.

Drainage Database

A 0.125° (−10 km) drainage database for the NSRB above Edmonton, was constructed using the Green Kenue tool [28] for MESH model input. It consists of 278 grid cells or Grouped Response Unit (GRU) and twelve land use CLASS types (Figure 2). A GRU-based approach combines regions of similar hydrological behavior in the whole drainage basin to simulate them together. Each GRU grid is represented by distinct tiles (landuse type) based on input from a Digital Elevation Model (DEM) from the Canadian Digital Elevation Data (CDED) at a scale of 30 m (1:50,000) (Figure 1a). The 30-metre land cover data (Figure 1b) from the Canada Center for Remote Sensing (CCRS, 2015) and the shapefiles of the catchment and rivers are available from the National Hydro Network—NHN—GeoBase Series.

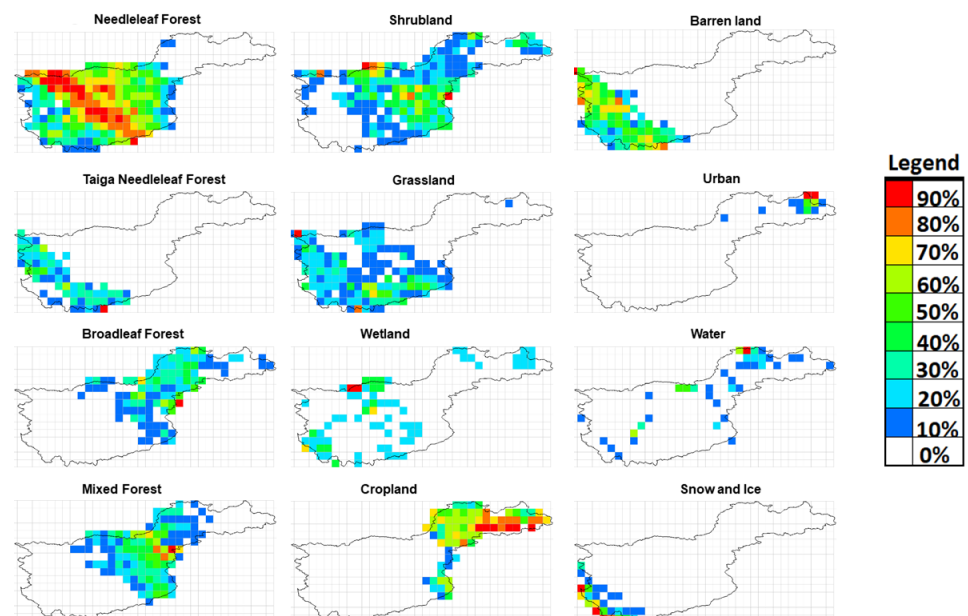


Figure 2. Twelve land use CLASS types and their fraction in each grid, used in the MESH Model of NSRB above Edmonton, AB, Canada.

2.3. Hydrological Data

The Edmonton hydrometric station (05DF001) recorded natural flows of the NSR before 1962. Construction of the Brazeau and Bighorn Dams was completed in 1963 and 1972, respectively. These hydroelectric facilities shift the seasonal distribution of stream discharge, but have a negligible influence on annual and peak flows at Edmonton. The River Forecast Centre of Alberta Environment and Parks computed natural flows at the reservoir sites and, by routing this runoff to Edmonton, produced a record of naturalized river flow. The daily naturalized streamflow record for the NSR at Edmonton from 1912–2010 was used in the calibration of the hydrological model and validation of model output.

In Figure 3, water year hydrographs are plotted for three time periods. This comparison of historical natural flows of the NSR at Edmonton shows a decrease in the warm season (May–September) in the past 30 years and increased flows in the cold season (October–April). The total annual flow increased by 3.46% for the period 1950–1979 and decreased by 5.29% for the period 1980–2009 compared to a baseline period of 1912–1941. The recent changes in total annual flows reflect increased temperature and decreased snowpack.

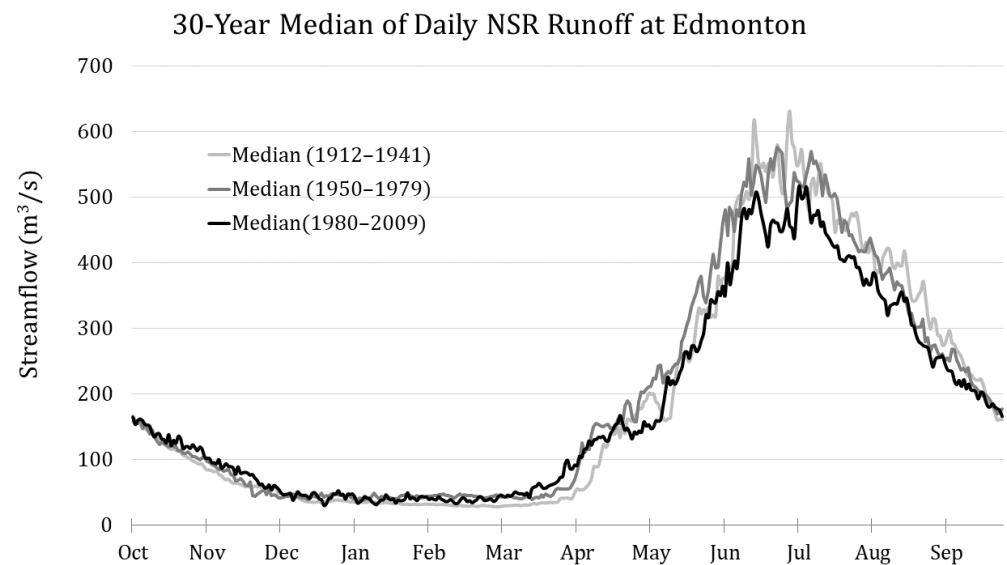


Figure 3. Comparison of median of 30-year daily natural streamflow for the NSR at Edmonton, AB, Canada for three time periods.

Detection and attribution of climate cycles are necessary to distinguish natural climate variability from trends imposed by global climate change. The wavelet transformation [29] of time series assigns power to the spectrum of frequencies across the time domain. Figure 4 is a continuous wavelet plot for NSR natural streamflow at Edmonton from 1911–2010. The power at high frequencies (2–4 years) demonstrates the strong effect of the El Niño Southern Oscillation (ENSO) in this region. There is also an indication of decadal variability (8–32 years), which corresponds to the frequency of the Pacific Decadal Oscillation (PDO).

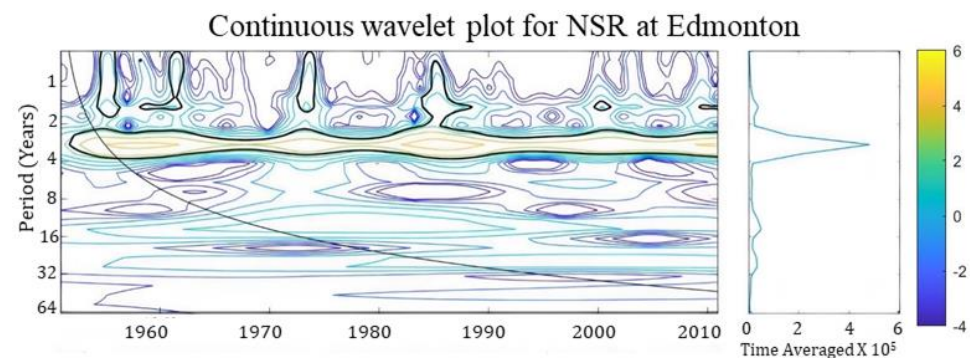


Figure 4. Continuous wavelet plot for NSR natural streamflow at Edmonton, AB, Canada from 1950–2010.

2.4. Forcing Data

2.4.1. Historical Climate Data

The MESH hydrological model was forced with the historical (1979–2016) gridded meteorological data of bias-corrected WFDEI-GEM-CaPA with spatiotemporal resolution of three-hourly $\times 0.125^\circ$ (~ 10 km) [30,31]. The drainage area of the NSR at Edmonton was masked out for seven forcing variables (incoming shortwave radiation, incoming longwave radiation, precipitation rate, air temperature, wind speed, barometric pressure, and specific humidity) required to run the MESH Land Surface hydrological model.

The WFDEI-GEM-CaPA data set is a combination of the forcing variables from the Global Environmental Multiscale (GEM) atmospheric model, the Canadian Precipitation Analysis (CaPA) and the EU WATCH ERA-Interim reanalysis (WFDEI). A multivariate generalization of the quantile mapping methodology (MBCn, [32]) was performed to bias-

correct the WFDEI against GEM-CaPA at $3\text{ h} \times 0.125^\circ$ resolution during the overlapping period (2005–2016), and hindcasting was performed back to 1979 for the final WFDEI-GEM-CaPA product.

2.4.2. Future Climate Data

This study used an ensemble of 15 initial condition simulations from the CanRCM4 under the RCP 8.5 high emission scenario [33]. The three-hourly 15-member ensemble of medium resolution (0.44°) extends from 1950 to 2100. It was bias-corrected using historical gridded meteorological data WFDEI-GEM-CaPA as described in [30] (2020). The resulting bias-corrected dataset at resolutions of 3-h and 0.125° is a consistent set of intra-model climate projections suitable for large-scale uncertainty modeling and constructing future climate scenarios.

3. Methods of Statistical Analysis and MESH Model Optimization

3.1. Statistical Analysis

The non-parametric Mann-Kendall (MK) test and Sen's slope estimator were used to detect trends in the climate forcing data (T_{\max} , T_{\min} , and Pr) as well as in runoff. The MK statistic (S), normalized test statistics (Z), and measure of the probability (p -value), were calculated for each climate forcing data. A small absolute value of S indicates no trend. A large positive/negative S value indicates an upward/downward trend; however, the associated probability (p -value) is necessary to statistically quantify the significance of the trend. For each variable, the Sen's slope estimator finds all possible linear slopes, ranks the slope estimates, and gives the median and its 95% confidence interval. Furthermore, for the evaluation of "Goodness-of-Fit" measures in the observed and simulated flows, the Nash–Sutcliffe Efficiency (NSE), natural log of NSE ($\ln NSE$), percentage error (PERR), percentage of model bias (PBIAS), coefficient of determination (R^2) and root mean square error to standard deviation ratio (RSR) were calculated for model assessment.

3.2. MESH Model Optimization

Most of the MESH model parameters are taken from CLASS technical documentation [23] and literature review [25,34,35]. The sensitive parameters used in this study are adopted from the analysis conducted by [35]. The MESH model was coupled with the OSTRICH optimization and parameter estimation toolkit [36] for Multi-Objective optimization using the PADDs (Pareto Archived Dynamically Dimensioned Search) algorithm. The objective function consists of weighted values of Nash–Sutcliffe efficiency (NSE) for peak flows, natural log of Nash–Sutcliffe efficiency ($\ln NSE$) for low flows and percentage of bias (PBIAS) for volume correction. Four types of parameters were calibrated: vegetation, soil, hydraulics, and hydrology properties (Table 1). The simulation with the lowest objective function value of 0.014 was used for validation and the projection of future flows.

Table 1. Parameters used in the calibration process for each CLASS type and hydrology using OSTRICH optimization toolkit.

Parameters Type	Variable	Description	Lower Limit	Upper Limit
Vegetation Parameters	LNZ0	Natural logarithm of the roughness length	−3.0	0.90
	LAMX	Annual maximum leaf area index	3.0	6.0
	ALVC	Average visible albedo when fully leafed	0.04	0.2
	RSMN	Minimum stomatal resistance	60	110
	CMAS	Annual maximum canopy mass	2.0	10.0

Table 1. Cont.

Parameters Type	Variable	Description	Lower Limit	Upper Limit
	ROOT	Annual maximum root depth	0.2	4.0
	QA50	Reference value of shortwave radiation	10.0	50.0
	VPDA	Vapor pressure deficit coefficient "A"	0.2	0.8
	VPDB	Vapor pressure deficit coefficient "B"	0.7	1.3
	MANN	Manning's 'n'	0.02	2.0
Soil Hydraulic Parameters	SDEP	Depth of the soil column	0.1	4.1
	DDEN	Drainage density	2.0	100.0
	KSAT	Saturated surface soil conductivity	0.001	0.01
Soil Texture Parameters	CLAY	Percent content of clay in the mineral soil	10.0	50.0
	SAND	Percent content of sand in the mineral soil	10.0	50.0
Hydrology Parameters	R2N	Channel Manning	0.02	0.5
	R1N	Overbank Manning	0.02	0.5
	PWR	Baseflow exponent of lower zone function	0.6	3.0
	FLZ	Baseflow lower zone function	6.0×10^{-6}	6.0×10^{-3}

4. Results

4.1. Climate Projections

A detailed explanation of changes in temperature and precipitation and their extremes is necessary to understand the ongoing future impact of climate change on NSRB and its consequences for changes of dynamics of hydrology and shifts in the snowmelt period.

4.1.1. Projected Changes in Near/Far Future Climates

From the ensemble of 15 initial-condition CanRCM4 (RCP 8.5) simulations of the climate of the NSRB above Edmonton, we computed the mean annual and seasonal differences in temperature and precipitation between the baseline period (1980–2010) and near (2021–2050) and far future (2051–2080). Figure 5 shows the mean annual and seasonal climate changes. There is an increase in mean annual temperature of around 2 °C in the near future and 4 °C in the far future. The intra-model variability in precipitation is higher in the far future (20.5%) compared to the near future (11.8%). The largest increases in minimum temperatures, exceeding 6 °C in the far future, occur in winter. The rise in maximum temperatures is largest in summer. Precipitation is increasing in all seasons except summer; when there are both drier and wetter ensemble projections. There is much less intra-model variability in precipitation in summer than in the other three seasons.

Table 2 is a summary of the annual and seasonal changes in minimum temperature, maximum temperature, and precipitation for the mean of the 15-ensemble initial condition simulations from CanRCM4 (RCP 8.5) for the near and far future for the NSRB above Edmonton. The ensemble means show that the winter minimum temperature and summer maximum temperature are increasing at a much higher rate compared to the other seasons. Similarly, an increase in the ensemble mean precipitation is higher in spring and fall compared to the summer and winter.

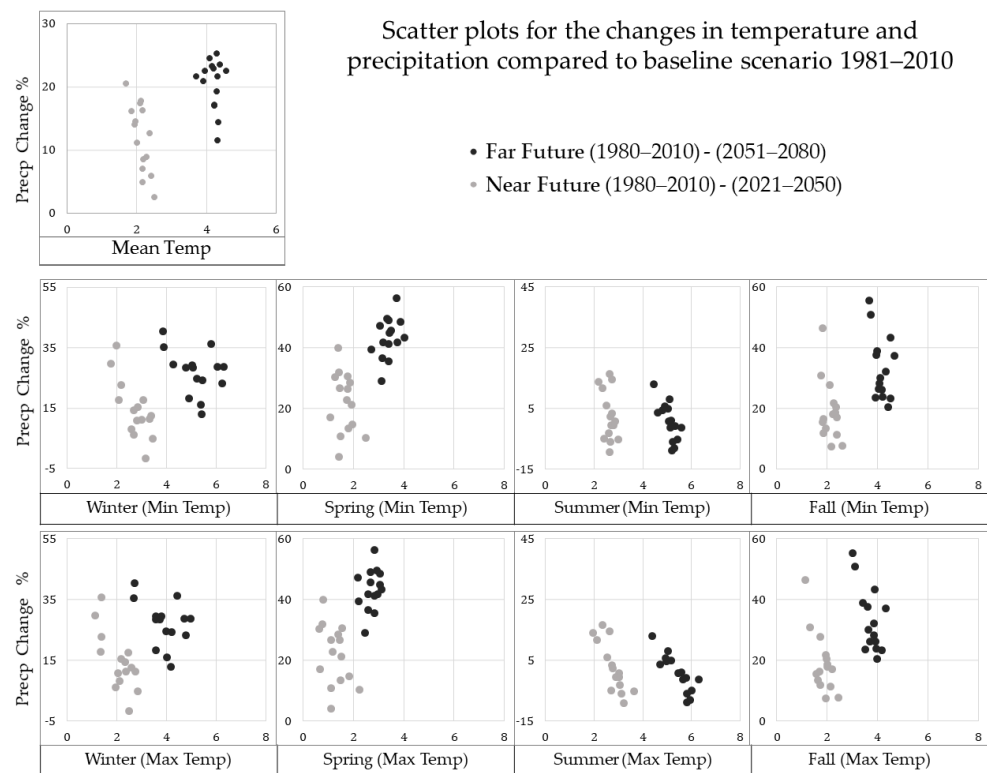


Figure 5. Mean and seasonal changes in temperature and precipitation change from the ensemble of 15 initial condition simulations from CanRCM4 and the RCP8.5 scenario for the NSRB above Edmonton, AB, Canada.

Table 2. Summary of annual and seasonal changes in minimum temperature (Tmin), maximum temperature (Tmax), and precipitation (Precp) for the mean of the 15-member ensemble of initial-condition simulations from CanRCM4 (RCP8.5) scenario for near and far future for the NSRB above Edmonton. The largest climate changes are highlighted in bold.

	Near Future (1981–2010)-(2021–2050)			Far Future (1981–2010)-(2051–2080)		
	Tmin	Tmax	Precp (%)	Tmin	Tmax	Precp (%)
Annual	2.28	1.99	11.85	4.45	3.95	20.50
Winter	2.72	2.08	14.38	5.17	3.92	26.92
Spring	1.66	1.26	21.90	3.41	2.74	43.32
Summer	2.63	2.78	2.59	5.09	5.44	0.62
Fall	2.12	1.83	18.89	4.15	3.72	33.13

4.1.2. Projected Changes in Annual and Seasonal Precipitation

A time series of seasonal and annual precipitation (1951–2100) produced by the 15-member CanRCM4 ensemble (RCP 8.5) in Figure 6 shows that the intra-model variability increases over time toward the end of the century around a rising linear trend and ensemble median. Seasonal time series indicate that spring has the highest increasing trend as the wettest months shift to earlier in the year. Summer has a decreasing trend and highest intra-model variability with a large range between wet and dry years.

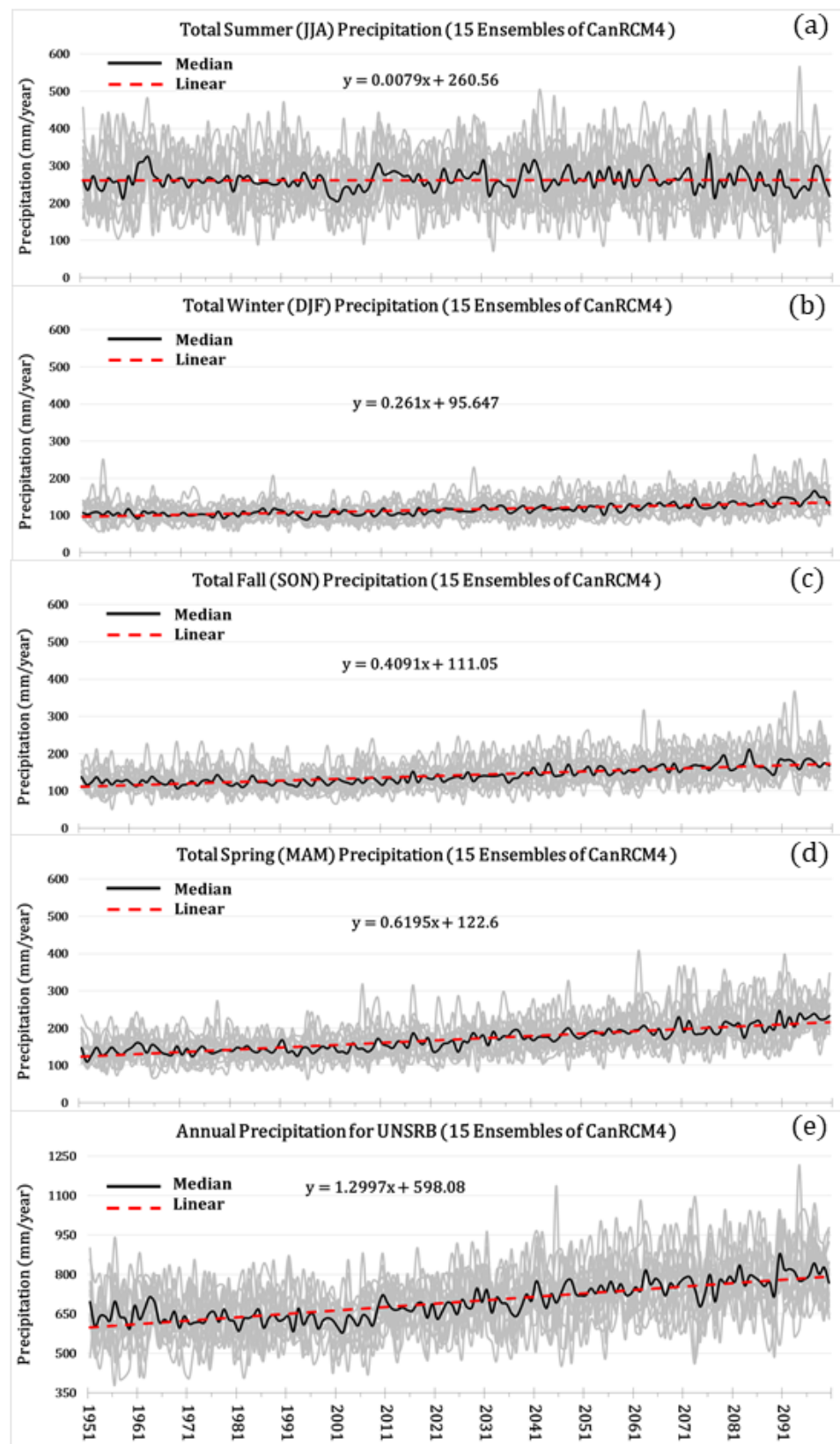


Figure 6. Times series (1951–2100) of seasonal (a–d) and total annual (e) precipitation for the 15-member CanRCM4 ensemble (RCP 8.5). The ensemble median (black) and linear trend (red) are shown.

Table 3 gives the results of the non-parametric Mann-Kendall (MK) test and Sen's slope estimator for annual and seasonal precipitation and maximum and minimum temperature averaged for the 15-member ensemble of bias-corrected data from CanRCM4 (RCP8.5) for the period 1951–2100. The MK test reveals the trend and Sen's slope estimates the trend magnitude with a significance level of 0.05. Summer precipitation shows no trend and fall minimum temperature has a decreasing trend. Otherwise, there is an increasing trend in all temperature and precipitation variables.

Table 3. The results of a non-parametric Mann-Kendall (MK) test and Sen's slope estimator for average annual and seasonal precipitation, and maximum and minimum temperature for a 15-member ensemble of bias-corrected data from CanRCM4 (RCP8.5) from 1951–2100.

		MK Trend Test	MK Statistic	Normalized Test Statistic	p-Value	Sen's Slope	95% Confidence Interval	
			(S)	(Z)			Min	Max
Precp	Annual	Increasing	7163	11.64	2.20×10^{-16}	1.3421	1.2061	1.4730
	Winter	Increasing	6595	10.72	2.20×10^{-16}	0.2510	0.2161	0.2870
	Spring	Increasing	7837	12.73	2.20×10^{-16}	0.6177	0.5586	0.6708
	Summer	No trend	−25	−0.04	0.9689	−0.0026	−0.0997	0.1016
	Fall	Increasing	7317	11.89	2.20×10^{-16}	0.4030	0.3600	0.4491
Tmax	Annual	Increasing	269,116	10.57	2.20×10^{-16}	0.0042	0.0036	0.0049
	Winter	Increasing	917	3.19	0.0014	0.0164	0.0066	0.0282
	Spring	Increasing	425	1.48	0.1395	0.0118	−0.0030	0.0321
	Summer	Increasing	1065	3.71	0.0002	0.0221	0.0121	0.0315
	Fall	Increasing	351	1.22	0.2225	0.0117	−0.0105	0.0294
Tmin	Annual	Increasing	304,433	11.95	2.00×10^{-17}	0.0049	0.0042	0.0055
	Winter	Increasing	101	0.35	0.7274	0.0021	−0.0094	0.0127
	Spring	Increasing	593	2.06	0.0391	0.0146	0.0005	0.0339
	Summer	Increasing	1175	4.09	4.28×10^{-5}	0.0197	0.0110	0.0290
	Fall	Decreasing	−152	−0.53	0.5987	−0.0035	−0.0222	0.0105

4.1.3. Projected Changes in Extreme Temperature and Precipitation

Changes in extreme temperature and precipitation are evident in the probability distribution functions (PDFs) in Figure 7. The PDFs are plotted for daily precipitation and maximum/minimum and mean temperature and for summer and winter for contrasting 60-year baseline (1951–2010) and future (2041–2100) periods. The bias-corrected CanRCM4 (RCP 8.5) data was fitted with a normal distribution. The PDF of daily precipitation shows wetter conditions in future with higher intensity rainfalls. There is a clear shift in the PDFs towards higher future mean temperatures; however, a shift in the tails of the distributions differs between seasons, with increased minimum temperatures in winter and higher maximum temperatures in summer.

4.2. MESH Modeling and Future Flows of NSRB at Edmonton

The optimized parameter values from OSTRICH were used to calibrate the MESH model using 3-hourly $\times 0.125^\circ$ (−10 km) observed historical gridded meteorological data for the period February 1995 to December 2002. The same forcing data were used to validate the model at daily intervals from January 2003 to December 2010. The calibrated MESH model was then used to simulate future flows of the NSR at Edmonton from 1951 to 2100 using 3-hourly $\times 0.125^\circ$ (−10 km) bias-corrected forcing data from a 15-member ensemble of CanRCM4 (RCP8.5).

Projected Changes in Probability Distribution Function's of Temperature and Precipitation

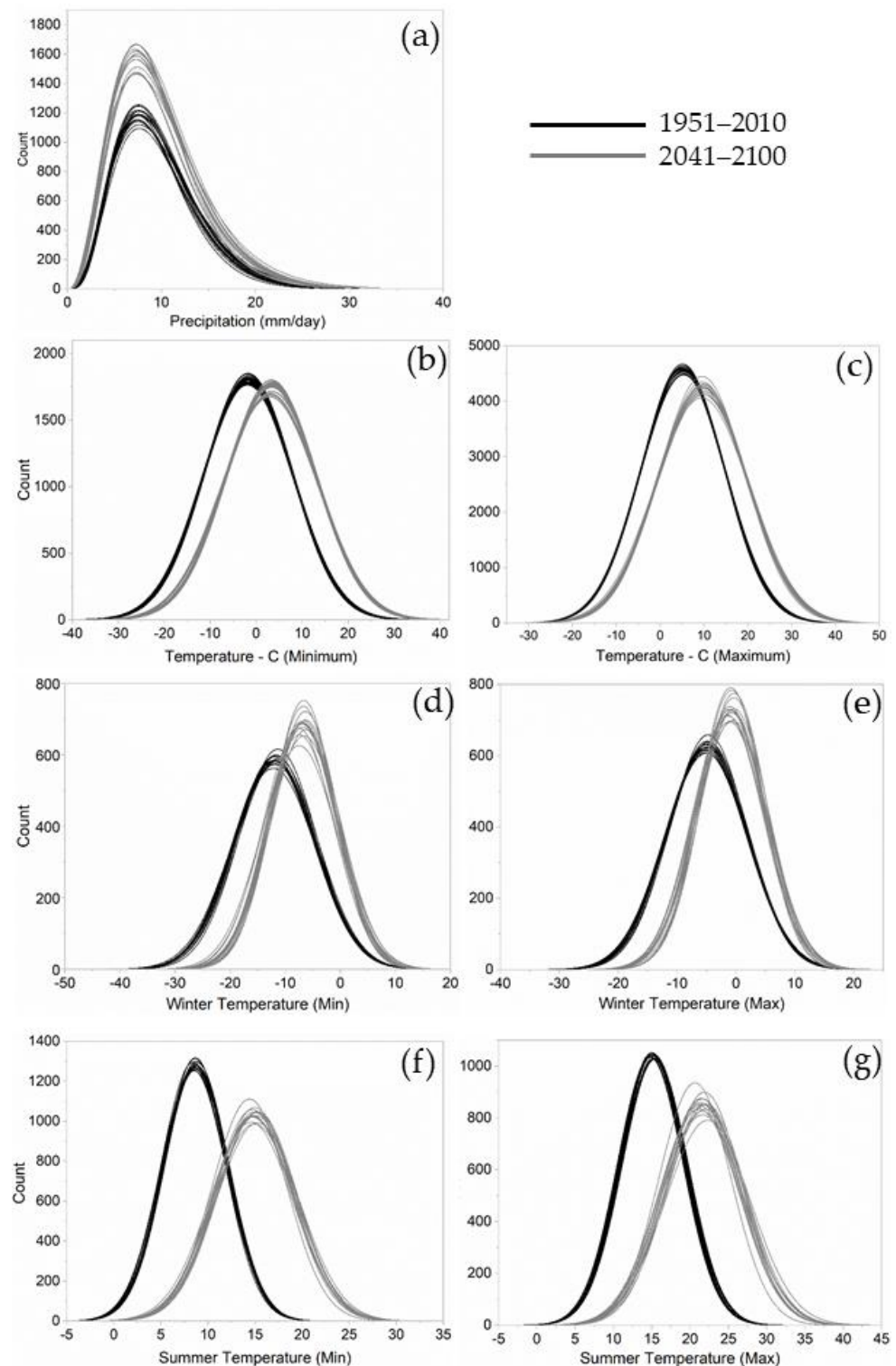


Figure 7. The PDFs of the daily precipitation (a) and minimum/maximum temperature per day and for the summer/winter seasons (b–g) for contrasting 60-year baseline (1951–2010) and future (2041–2100) periods. The bias-corrected CanRCM4 (RCP 8.5) data were fitted with a normal distribution.

4.2.1. Calibration and Validation of the MESH Model

The MESH hydrological model was calibrated and validated on naturalized streamflow at Edmonton using the bias-corrected WFDEI-GEM-CaPA historical gridded forcing data. Figure 8 is a plot of observed and simulated daily flow of the NSR at Edmonton for calibration and validation periods. Table 4 gives statistics for goodness of fit. The calibration Nash–Sutcliffe efficiency (NSE) of 0.69 indicates good agreement between modeled and observed flows. The overall performance of model dynamics and the seasonal variability in river flow is captured well by the MESH model with a percentage bias of 7.04, indicating a strong relationship between simulated and observed flows. MESH provides a close fit to the observed flows for the calibration period (February 1995–December 2002), while for the independent validation period (January 2003–December 2010) the performance of the MESH model is reduced. The reduction is, however, limited and the model is able to maintain a very good representation of the overall water balance and the inter-annual and seasonal dynamics.

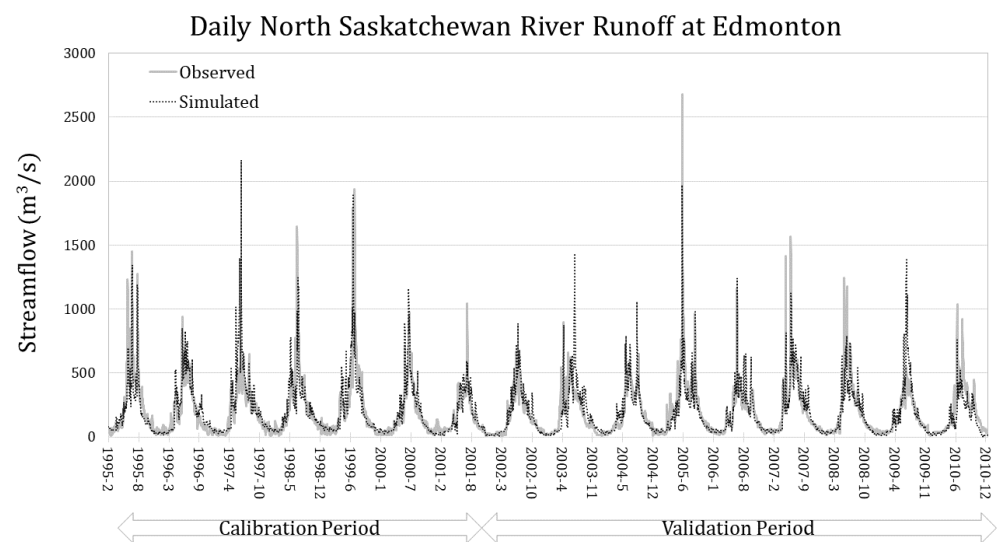


Figure 8. Comparison of observed and simulated daily runoff of NSR at Edmonton for calibration (February 1995–December 2002) and validation (January 2003–December 2010) periods.

Table 4. Goodness of fit results for the calibration and validation of the MESH modeling of the flow of the NSR at Edmonton.

Goodness-of-Fit	Calibration (February 1995–December 2002)	Validation (January 2003–December 2010)
Nash–Sutcliffe efficiency (NSE)	0.69	0.67
Log of Nash–Sutcliffe efficiency (lnNSE)	0.50	0.32
Percent error (PERR)	4.11	−2.25
Percent model bias (PBIAS)	4.11	2.25
Coefficient of determination (R ²)	0.72	0.68
RMSE-to-SD Ratio (RSR)	0.56	0.59

4.2.2. Projected Changes in Streamflow

The future flows of the NSR at Edmonton were simulated using bias-corrected data from 15 runs of the Canadian Regional Climate Model (CanRCM4) under the RCP 8.5 emission scenario ([30,33]). Figure 9a is a plot of MESH simulated mean annual runoff at Edmonton from 1951–2100. This ensemble of time series exhibits large variability around an upward trending ensemble mean, with an increasing range between high and low flows toward the end of the 21st century. These results are based on the future climate from the CanRCM4 dynamical downscaling of the Canadian Earth System Model (CanESM2). The

use of a single pairing of ESM/RCM and one RCP enables us to control for uncertainty due to the use of different models and greenhouse gas emission scenarios. Thus, differences among streamflow projections represent uncertainty related to the natural variability of the regional hydroclimate in a warming climate.

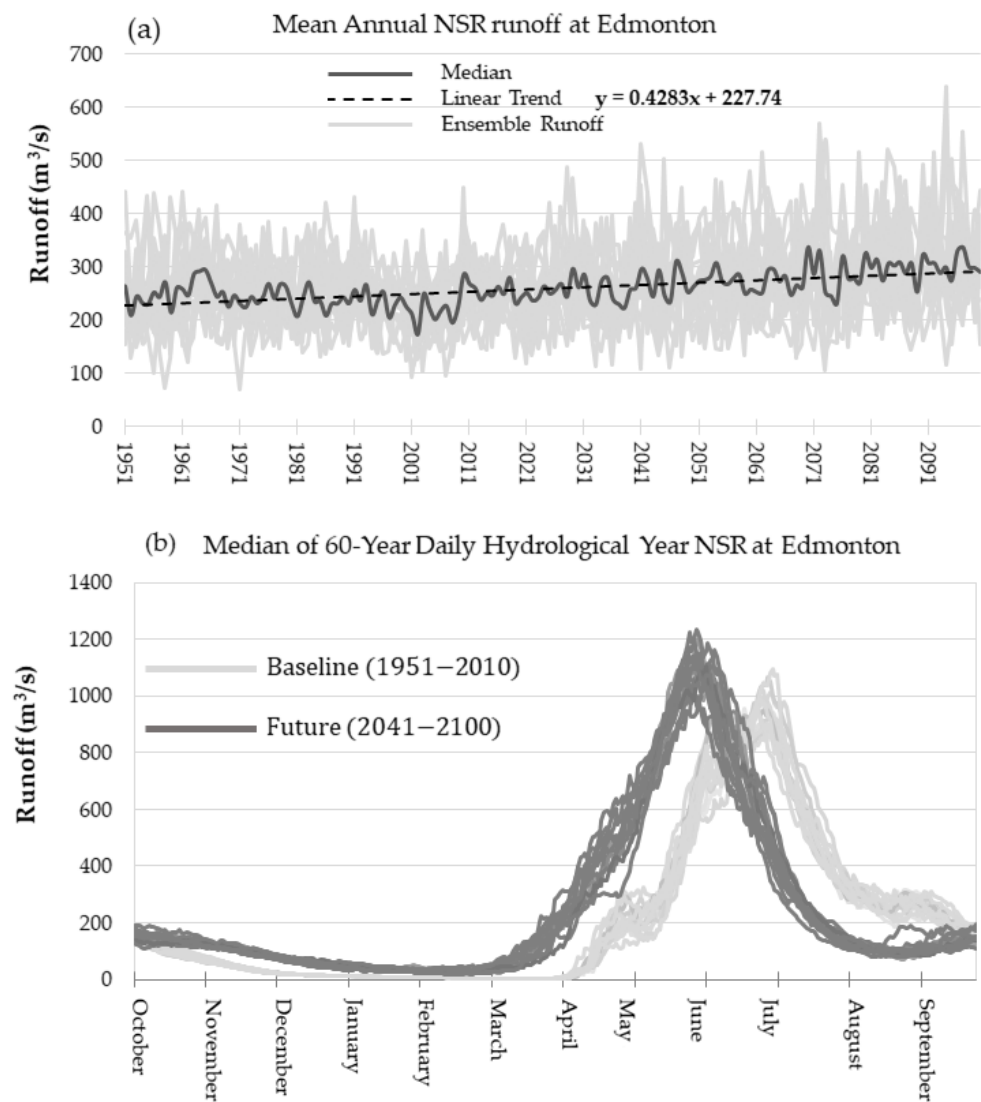


Figure 9. (a) MESH simulated mean annual runoff of the NSR at Edmonton from 1951–2100. (b) Comparison of median 60-year daily NSR flow at Edmonton for baseline (1951–2010) and future (2041–2100) periods. These hydrographs were generated using the MESH hydrological model run with the 15-member ensemble of bias-corrected CanRCM4 forcing data (RCP8.5).

Figure 9b is a plot of the annual water-year hydrograph for the baseline (1951–2010) and future (2041–2100) periods derived from the MESH model run. It shows a shift in annual peak flows occurring approximately one-month earlier in the year, with higher winter flows and lower summer flows. The minor peak in late April to early May in the historical hydrograph is not apparent in the future flows. This suggests that at lower elevations, the landscape no longer contributes significant runoff in a warmer climate. A shoulder of sustained flow in September in the historical hydrograph also disappears, as future river flow steeply declines in summer. Table 5 shows the summary of annual and seasonal changes in median runoff. There is an increase of 19% annual average runoff for the future period (2041–2100) compared to the baseline period (1951–2010) given an increase in future precipitation. Similarly, runoff is increased in every season except in

summer. There is a dominant increase in winter and spring runoff due to more precipitation and early snowmelt.

Table 5. Summary of annual and seasonal changes in median runoff simulated by MESH using a 15-member ensemble of bias-corrected forcing data from CanRCM4 (RCP8.5) for base period (1951–2010) and future period (2041–2100).

RUNOFF	Base Period (1951–2010)	Future Period (2041–2100)	% Change
Annual	927.79	1104.55	19.05
Winter	11.69	57.07	388.21
Spring	164.52	443.49	169.57
Summer	619.27	469.05	−24.26
Fall	132.31	134.94	1.98

Table 6 gives the results of a non-parametric Mann-Kendall (MK) test and Sen’s slope estimator for median annual and seasonal runoff simulated by MESH using the 15-member ensemble of forcing data from CanRCM4 (RCP 8.5) from 1951–2100. There is an increasing trend in annual runoff; however, the seasonal runoff is increasing in winter and spring, but decreases in summer and fall.

Table 6. The results of a non-parametric Mann-Kendall (MK) test and Sen’s slope estimator for median annual and seasonal runoff simulated by MESH using a 15-member ensemble of bias-corrected forcing data from CanRCM4 (RCP 8.5) from 1951–2100.

RUNOFF	MK Trend Test	MK Statistic	Normalized Test Statistic	p-Value	Sen’s Slope	95% Confidence Interval	
						(S)	(Z)
Annual	Increasing	4585	7.45	9.41×10^{-14}	0.4277	0.3256	0.5277
Winter	Increasing	9339	15.17	2.20×10^{-16}	0.4087	0.3586	0.4639
Spring	Increasing	8801	14.30	2.20×10^{-16}	2.9701	2.7070	3.2243
Summer	Decreasing	−6709	−10.90	2.20×10^{-16}	−1.8512	−2.0956	−1.6151
Fall	Decreasing	−585	−0.95	0.3426	−0.0478	−0.1386	0.0479

4.2.3. Projected Changes in Extreme Streamflow

The ensemble of probability distributions derived from 15 runs of MESH is plotted for the baseline (1951–2010) and future (2041–2100) periods. In Figure 10, the frequency of daily mean and high/low flows are shown by fitting a normal distribution to histograms of the daily mean and extreme flows of the NSR at Edmonton. A shift in probability toward higher flows (Figure 10a) reflects the projected climate changes, and specifically wetter conditions in winter and spring. The right tail of the distribution of future daily flows is extended. This higher probability of extreme flows is depicted in Figure 10b, where the frequency of flows exceeding $500 \text{ m}^3/\text{s}$ is plotted. The extreme flow PDFs have longer tails in the future period, indicating a much higher probability of flood events. The PDF of flows ($<500 \text{ m}^3/\text{s}$) in Figure 10c, suggests a decrease in frequency and an increase in magnitude.

The changes in the magnitude and timing of extreme flows are of the utmost importance and illustrated in Figure 11 using MESH and the 15-member ensemble of forcing data from CanRCM4 (RCP8.5) from 1951–2100. The change in timing of the peak and low flows is shown with colour coding of the months. Figure 11a shows a dramatic mid-21st century shift in the timing and magnitude of low flows. There is a large increase in the range of flows and the timing shifts from late winter to late summer and throughout the fall. As winter becomes wetter and snow turns into rain, winter is no longer the season of minimum flow, and rather the timing of low flows reflects the drier summers and loss of snow and ice at high elevations, which historically have maintained summer river levels.

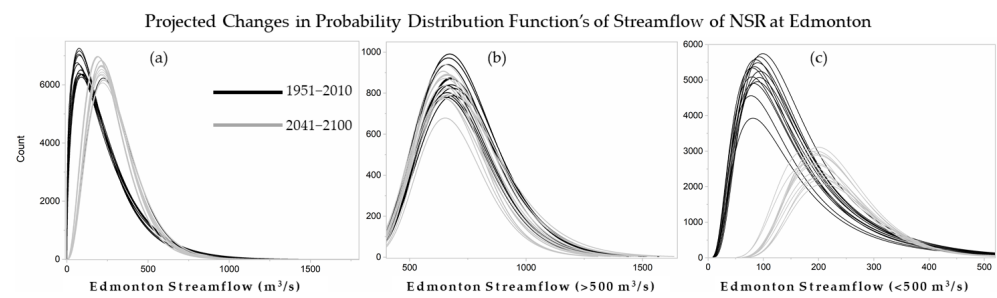


Figure 10. (a) Comparison of normal distributions fitted to the histograms of daily mean NSR flow. Comparison of frequency distributions of daily high (b) and low (c) flows of the NSR at Edmonton between a baseline from (1951–2010) and future (2041–2100) periods.

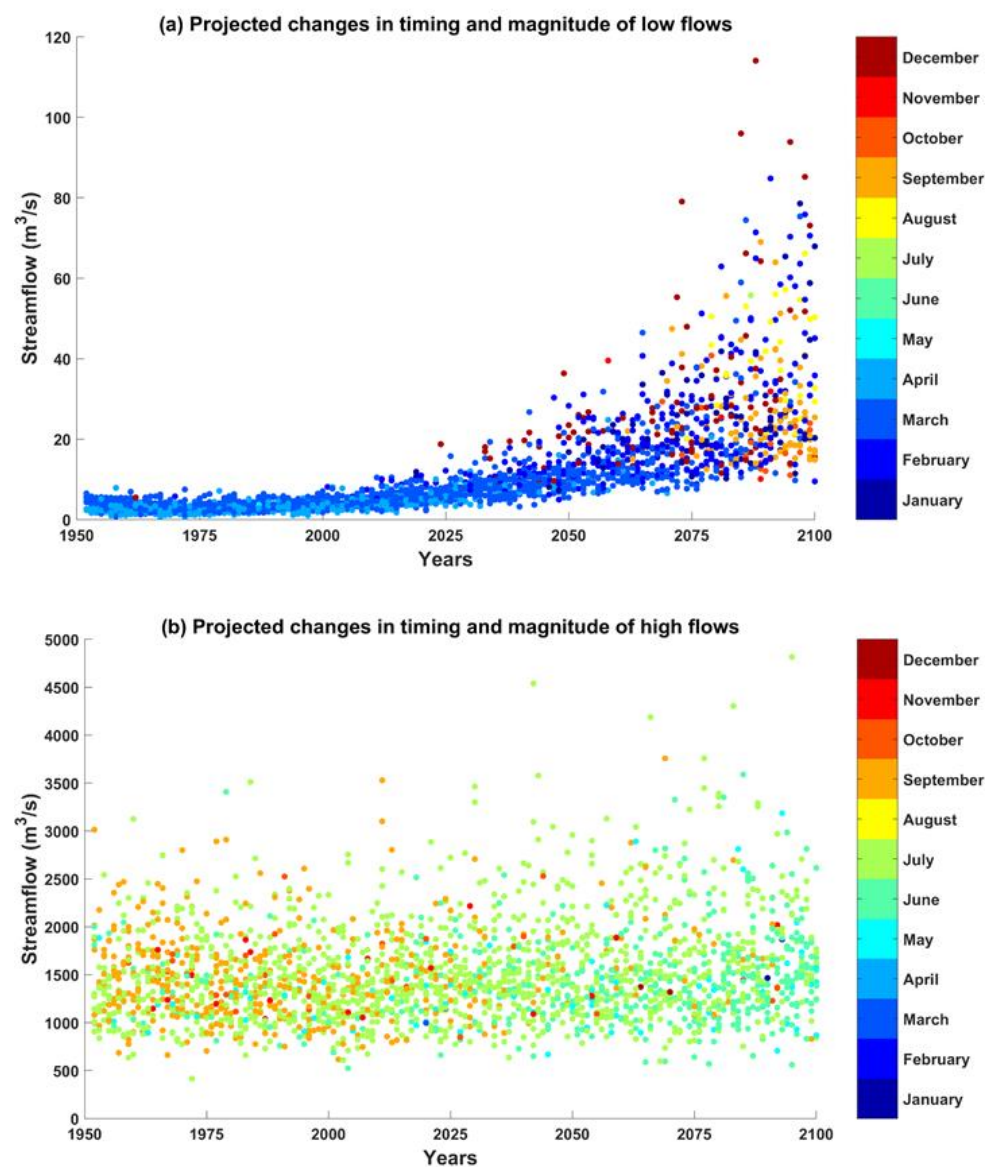


Figure 11. The magnitude and timing of daily low (a) and high (b) flows of the NSR at Edmonton derived from the MESH model run using the 15-member ensemble of bias-corrected data from CanRCM4 (RCP8.5).

Figure 11b suggests that the range of high flows also expands, with an unchanged minimum of about $500 \text{ m}^3/\text{s}$, but much higher values than in the past approaching $5000 \text{ m}^3/\text{s}$. The timing also shifts around mid-21st century with fewer maximum flows in late summer

and fall, and an increased frequency in spring. Whereas historically rainfall runoff combined with the summer melting of snow and glacier ice produced high flows, earlier peak runoff and lower summer river levels will favor springtime maximum annual flows.

5. Discussion

Our modeling and analysis of the future climate and hydrology of the North Saskatchewan River Basin (NSRB) gave results that have important implications for the availability, management, and use of surface water in the Edmonton metropolitan area. Most of the recent climate change in this region has been an increase in the lowest temperatures; minimum daily winter temperatures have increased by about 6 °C. There is no significant trend in the instrumental record of precipitation. Fluctuations in precipitation over the past 120 years are dominated by large differences between years and decades. Future projections from climate models suggest warmer and wetter weather in winter and spring and, on average, drier conditions in mid to late summer.

Uncertainty in hydrological ensemble projections showed unique responses to uncertainty in the precipitation and temperature ensembles. In response to these projected climate changes, the seasonal pattern of river flow will shift, with future river levels peaking about one month earlier during May. More precipitation falling as rain rather than snow, combined with advanced spring snow melt, will result in earlier peak streamflow. Cold season (winter and early spring) flows will be significantly higher, and the timing of maximum annual flows will shift from summer to spring. As a warming climate intensifies the hydrological cycle, the range of river levels will expand, with larger departures from a shifting baseline of higher winter flows and lower summer flows.

Lower river levels in June to August will have implications for surface water supplies during the season of the highest demand. Data from recent decades indicate that absolute water use and demand has increased but at a lesser rate than the increasing population of the Edmonton region [15]. As a result, there has been a decoupling of per capita water use from growth in the economy and population of the region. Whereas this more efficient use of water supplies represents an important adaptation to a changing climate, other adjustments to water policy, planning, and management will be required given the changes in climate and water supplies projected by our study.

Changes in the severity of extreme hydrological events, and in the seasonal distribution of water resources, will have major impacts on terrestrial and aquatic ecosystems, and on the availability of municipal and industrial water supplies [37,38]. Because water quality in the NSR is directly related to both runoff from the landscape and instream flows, it will be affected by climate change impacts on river flows and on runoff generated by precipitation and snowmelt. Higher concentrations of turbidity, colour, nutrients, and algae are anticipated because of increased precipitation, a larger range of flows in the NSR, floods, droughts, forest fires, and higher water temperatures.

6. Conclusions

Uncertainty in hydrological projections was much more intimately linked with uncertainty in the ensemble projections of precipitation compared to temperature, indicating, we must reduce uncertainty in precipitation data for improved modeling credibility. Both incremental long-term changes in water levels, and extreme fluctuations around the changing baseline, will have impacts requiring adaptation of water resource planning and policy. Our use of climate forcing data from an ensemble of runs of a CanRCM4 (RCP8.5) revealed the uncertainty in the future river hydrology that arises from the internal natural variability in the regional hydroclimate. Water allocation and the design of storage and conveyance structures are based mainly on average seasonal water levels, but otherwise water resources are managed to prevent the adverse impacts of flooding and drought. The operation, and possible structural integrity, of infrastructure for drainage, water supply, and treatment is vulnerable to climate change. Much of the risk is due to the expectation

of more intense precipitation, earlier snow melts, prolonged low water levels, and more extreme weather events.

Author Contributions: M.R.A. and D.J.S. planned this study and experiments; D.J.S. contributed to writing the manuscript and overall supervision of the project; M.R.A. conducted the modeling experiments, performed the analysis, and prepared the text and graphics for the manuscript; Both authors have read and agreed to the published version of the manuscript.

Funding: The research described in this paper was funded by EPCOR Utilities Ltd. and by the Natural Sciences and Engineering Research Council (NSERC) of Canada, grant number CRDPJ520747-17.

Institutional Review Board Statement: Not applicable.

Informed Consent Statement: Not applicable.

Data Availability Statement: The observed forcing data used in this study (WFDEI-GEM-CaPA, 1979–2016) for North America is freely available at the Federated Research Data Repository (<https://doi.org/10.20383/101.0111>). Bias-corrected CanRCM4 forcing data is freely available from the Federated Research Data Repository (<https://doi.org/10.20383/101.0230/>). The MESH model and OSTRICH are freely available from University of Saskatchewan Wiki webpage (<https://wiki.usask.ca/display/MESH/About+MESH>). All the script used in this study to analyze forcing data is also freely available at (<https://wiki.usask.ca/display/MESH/Forcing+Datasets+for+MESH>). All the statistics are computed in R using trend package. All the websites are last accessed on 2 September 2021.

Acknowledgments: The authors gratefully acknowledge the support of this research funded by EPCOR Utilities Ltd. and by the Natural Sciences and Engineering Research Council (NSERC) of Canada.

Conflicts of Interest: The authors declare no conflict of interest.

References

- Abbott, B.; Bishop, K.; Zarnetske, J.; Minaudo, C.; Chapin, F.; Krause, S.; Hannah, D.; Conner, L.; Ellison, D.; Godsey, S.; et al. Human domination of the global water cycle absent from depictions and perceptions. *Nat. Geosci.* **2019**, *12*, 533–540. [\[CrossRef\]](#)
- Jiménez Cisneros, B.E.; Oki, T.; Arnell, N.W.; Benito, G.; Cogley, J.G.; Döll, P.; Jiang, T.; Mwakalila, S.S. Freshwater Resources. In *Climate Change 2014: Impacts, Adaptation, and Vulnerability. Part A: Global and Sectoral Aspects. Contribution of Working Group II to the Fifth Assessment Report of the Intergovernmental Panel on Climate Change*; Field, C.B., Barros, V.R., Dokken, D.J., Mach, K.J., Mastrandrea, M.D., Bilir, T.E., Chatterjee, M., Ebi, K.L., Estrada, Y.O., Genova, R.C., et al., Eds.; Cambridge University Press: Cambridge, UK, 2014; pp. 229–269.
- Marvel, K.; Cook, B.; Bonfils, C.; Durack, P.; Smerdon, J.; Williams, A. Twentieth-century hydroclimate changes consistent with human influence. *Nature* **2019**, *569*, 59–65. [\[CrossRef\]](#)
- Bonsal, B.R.; Peters, D.L.; Seglenieks, F.; Rivera, A.; Berg, A. *Changes in Freshwater Availability across Canada. Chapter 6 in Canada's Changing Climate Report*; Bush, E., Lemmen, D.S., Eds.; Government of Canada: Ottawa, ON, Canada, 2019; pp. 261–342.
- Mudryk, L.; Derksen, C.; Howell, S.; Laliberté, F.; Thackeray, C.; Sospedra-Alfonso, R.; Vionnet, V.; Kushner, P.; Brown, R. Canadian snow and sea ice: Historical trends and projections. *Cryosphere* **2018**, *12*, 1157–1176. [\[CrossRef\]](#)
- Burn, D.; Abdul Aziz, O.; Pietroniro, A. A Comparison of Trends in Hydrological Variables for Two Watersheds in the Mackenzie River Basin. *Can. Water Resour. J./Rev. Can. Ressour. Hydr.* **2004**, *29*, 283–298. [\[CrossRef\]](#)
- Rood, S.; Samuelson, G.; Weber, J.; Wywrot, K. Twentieth-century decline in streamflows from the hydrographic apex of North America. *J. Hydrol.* **2005**, *306*, 215–233. [\[CrossRef\]](#)
- Donahue, W.; Allen, E.; Schindler, D. Impacts of Coal-Fired Power Plants on Trace Metals and Polycyclic Aromatic Hydrocarbons (PAHs) in Lake Sediments in Central Alberta, Canada. *J. Paleolimnol.* **2006**, *35*, 111–128. [\[CrossRef\]](#)
- St-Jacques, J.; Andreichuk, Y.; Sauchyn, D.; Barrow, E. Projecting Canadian Prairie Runoff for 2041–2070 with North American Regional Climate Change Assessment Program (NARCCAP) Data. *JAWRA J. Am. Water Resour. Assoc.* **2018**, *54*, 660–675. [\[CrossRef\]](#)
- Yip, Q.; Burn, D.; Seglenieks, F.; Pietroniro, A.; Soulis, E. Climate Impacts on Hydrological Variables in the Mackenzie River Basin. *Can. Water Resour. J./Rev. Can. Ressour. Hydr.* **2012**, *37*, 209–230. [\[CrossRef\]](#)
- Peters, D.; Atkinson, D.; Monk, W.; Tenenbaum, D.; Baird, D. A multi-scale hydroclimatic analysis of runoff generation in the Athabasca River, western Canada. *Hydrol. Process.* **2013**, *27*, 1915–1934. [\[CrossRef\]](#)
- Bawden, A.; Linton, H.; Burn, D.; Prowse, T. A spatiotemporal analysis of hydrological trends and variability in the Athabasca River region, Canada. *J. Hydrol.* **2014**, *509*, 333–342. [\[CrossRef\]](#)

13. Sauchyn, D.; Davidson, D.; Johnston, M.; Flannigan, M.; Fletcher, A.; Isaac, K.; Kulshreshtha, S.; Kowalczyk, T.; Mauro, I.; Pittman, J.; et al. The Prairie Provinces. In *Natural Resources Canada 2020, Canada in a Changing Climate: Advancing Our Knowledge for Action*; Natural Resources Canada: Ottawa, ON, Canada, 2020.
14. Golder Associates. *Water Supply Assessment for the North Saskatchewan River Basin*; North Saskatchewan Watershed Alliance: Edmonton, AB, Canada, 2008.
15. Anis, M.; Andreichuk, Y.; Kerr, S.; Sauchyn, D. Climate Change Risks to Water Security in Canada's Western Interior. In *Hydrological Aspects of Climate Change*; Pandey, A., Kumar, S., Eds.; Springer Transactions in Civil and Environmental Engineering; Springer: Singapore, 2021; pp. 25–60. ISBN 978-981-16-0394-5_2.
16. Kienzle, S.; Nemeth, M.; Byrne, J.; MacDonald, R. Simulating the hydrological impacts of climate change in the upper North Saskatchewan River basin, Alberta, Canada. *J. Hydrol.* **2012**, *412–413*, 76–89. [[CrossRef](#)]
17. Barrow, E.; Sauchyn, D. Uncertainty in climate projections and time of emergence of climate signals in the western Canadian Prairies. *Int. J. Climatol.* **2019**, *39*, 4358–4371. [[CrossRef](#)]
18. Sauchyn, D.; Vanstone, J.; Perez-Valdivia, C. Modes and Forcing of Hydroclimatic Variability in the Upper North Saskatchewan River Basin Since 1063. *Can. Water Resour. J./Rev. Can. Ressour. Hydr.* **2011**, *36*, 205–217. [[CrossRef](#)]
19. Sauchyn, D.; Vanstone, J.; St. Jacques, J.; Sauchyn, R. Dendrohydrology in Canada's western interior and applications to water resource management. *J. Hydrol.* **2015**, *529*, 548–558. [[CrossRef](#)]
20. Sauchyn, D.; Ilich, N. Nine Hundred Years of Weekly Streamflows: Stochastic Downscaling of Ensemble Tree-Ring Reconstructions. *Water Resour. Res.* **2017**, *53*, 9266–9283. [[CrossRef](#)]
21. Tennant, C.; Menounos, B. Glacier change of the Columbia Icefield, Canadian Rocky Mountains, 1919–2009. *J. Glaciol.* **2013**, *59*, 671–686. [[CrossRef](#)]
22. Pietroniro, A.; Fortin, V.; Kouwen, N.; Neal, C.; Turcotte, R.; Davison, B.; Verseghy, D.; Soulis, E.; Caldwell, R.; Evora, N.; et al. Development of the MESH modelling system for hydrological ensemble forecasting of the Laurentian Great Lakes at the regional scale. *Hydrol. Earth Syst. Sci.* **2007**, *11*, 1279–1294. [[CrossRef](#)]
23. Verseghy, D.; McFarlane, N.; Lazare, M. Class—A Canadian land surface scheme for GCMS, II. Vegetation model and coupled runs. *Int. J. Climatol.* **1993**, *13*, 347–370. [[CrossRef](#)]
24. Verseghy, D. Class—A Canadian land surface scheme for GCMS. I. Soil model. *Int. J. Climatol.* **2007**, *11*, 111–133. [[CrossRef](#)]
25. Mekonnen, M.; Wheeler, H.; Ireson, A.; Spence, C.; Davison, B.; Pietroniro, A. Towards an improved land surface scheme for prairie landscapes. *J. Hydrol.* **2014**, *511*, 105–116. [[CrossRef](#)]
26. Soulis, E.; Snelgrove, K.; Kouwen, N.; Seglenieks, F.; Verseghy, D. Towards closing the vertical water balance in Canadian atmospheric models: Coupling of the land surface scheme class with the distributed hydrological model watflood. *Atmos.-Ocean.* **2000**, *38*, 251–269. [[CrossRef](#)]
27. Kouwen, N.; Soulis, E.; Pietroniro, A.; Donald, J.; Harrington, R. Grouped Response Units for Distributed Hydrologic Modeling. *J. Water Resour. Plan. Manag.* **1993**, *119*, 289–305. [[CrossRef](#)]
28. *Green Kenue Reference Manual*; Canadian Hydraulics Centre of the National Research Council: Ottawa, ON, Canada, 2010.
29. Torrence, C.; Compo, G. A Practical Guide to Wavelet Analysis. *Bull. Am. Meteorol. Soc.* **1998**, *79*, 61–78. [[CrossRef](#)]
30. Asong, Z.; Elshamy, M.; Princz, D.; Wheeler, H.; Pomeroy, J.; Pietroniro, A.; Cannon, A. High-resolution meteorological forcing data for hydrological modelling and climate change impact analysis in the Mackenzie River Basin. *Earth Syst. Sci. Data.* **2020**, *12*, 629–645. [[CrossRef](#)]
31. Asong, Z.; Wheeler, H.; Pomeroy, J.; Pietroniro, A.; Elshamy, M. *WFDEI-GEM-CaPA: A Bias-Corrected 3-hourly 0.125 Gridded Meteorological Forcing Data Set (1979–2016) for Land Surface Modeling in North America*; Federated Research Data Repository: Saskatoon, SK, Canada, 2018.
32. Cannon, A. Multivariate quantile mapping bias correction: An N-dimensional probability density function transform for climate model simulations of multiple variables. *Clim. Dyn.* **2017**, *50*, 31–49. [[CrossRef](#)]
33. Scinocca, J.; Kharin, V.; Jiao, Y.; Qian, M.; Lazare, M.; Solheim, L.; Flato, G.; Biner, S.; Desgagne, M.; Dugas, B. Coordinated Global and Regional Climate Modeling. *J. Clim.* **2015**, *29*, 17–35. [[CrossRef](#)]
34. Davison, B.; Pietroniro, A.; Fortin, V.; Leconte, R.; Mamo, M.; Yau, M. What is Missing from the Prescription of Hydrology for Land Surface Schemes? *J. Hydrometeorol.* **2016**, *17*, 2013–2039. [[CrossRef](#)]
35. Haghnegahdar, A.; Razavi, S.; Yassin, F.; Wheeler, H. Multicriteria sensitivity analysis as a diagnostic tool for understanding model behaviour and characterizing model uncertainty. *Hydrol. Process.* **2017**, *31*, 4462–4476. [[CrossRef](#)]
36. Matott, L. *OSTRICH: An Optimization Software Tool, Documentation and User's Guide; Version 17.12.19*; University at Buffalo Center for Computational Research: New York, NY, USA, 2017; 79p.
37. Fyfe, J.; Derksen, C.; Mudryk, L.; Flato, G.; Santer, B.; Swart, N.; Molotch, N.; Zhang, X.; Wan, H.; Arora, V.; et al. Large Near-Term Projected Snowpack Loss over the Western United States. *Nat. Commun.* **2017**, *8*, 14996. [[CrossRef](#)] [[PubMed](#)]
38. Sturm, M.; Goldstein, M.; Parr, C. Water and life from snow: A trillion dollar science question. *Water Resour. Res.* **2017**, *53*, 3534–3544. [[CrossRef](#)]